Optical Appearance of Dynamical Models for Circumstellar Dust Shells around Long–period Variables: AFGL 3068

JAN MARTIN WINTERS[1], AXEL J. FLEISCHER[1],
THIBAUT LE BERTRE[2], ERWIN SEDLMAYR[1],

[1] Institut f. Astronomie & Astrophysik, TU Berlin, Berlin, Germany
[2] Observatoire de Paris, DEMIRM, Paris, France

Poster contribution presented at the IAU Symp. 177: *The Carbon Star Phenomenon*, May 27–31 1996, Antalya, Turkey

1 INTRODUCTION

Carbon stars on the Asymptotic Giant Branch are known to be places of copious dust formation accompanied by a substantial mass loss. The contribution of these stars to the replenishment of the Interstellar Medium (ISM) is uncertain but could be of the order of 0.5 $M_\odot\,yr^{-1}$ (Epchtein et al. 1990). Whatsoever, they certainly dominate the ISM enrichment in carbon–rich material over WC Wolf–Rayet stars or C–type Planetary Nebulae and thus play an important rôle in the chemical evolution of the Galaxy.

With the advent of Infrared (IR) surveys, unidentified IR sources have been discovered and some have been found to consist of heavily obscured carbon stars. For these extreme carbon stars (ECS) the large optical depth points to a process of mass loss at a huge rate ($\dot{M} \geq 10^{-5}\,M_\odot\,yr^{-1}$). They may thus contribute significantly to the supply of carbon–rich material in the ISM (Kastner et al. 1993). By their extreme properties ECS allow to probe the models of carbon dust formation and dynamics.

The best studied ECS is actually **GL 3068**. It is a long–period variable (P$\sim$ 700 days). Its broad band spectrum mimics that of a blackbody at $\sim$ 300 K (Jones et al. 1978). An absorption around 11.3 μm can be seen in its Low Resolution Spectrum (LRS, IRAS 1986). The detection of carbon–rich molecules such as HCN, HC_3N, etc. (Bujarrabal et al. 1994) supports the conclusion that GL 3068 has a carbon–rich circumstellar shell.

2 MODELING METHOD

We present a consistent time–dependent model for the circumstellar dust shell (CDS) around **GL 3068**, including a detailed treatment of hydrodynamics, thermodynamics, equilibrium chemistry, formation, growth and evaporation of carbon grains, and radiative transfer. We consider a spherically symmetric atmosphere surrounding a pulsating red giant, characterized by its mass $M_\star$, effective temperature $T_\star$, luminosity $L_\star$, pulsation period P, and the photospheric element abundances $\epsilon_{\rm i}$. In order to simulate the interior pulsation of the star, we apply a sinusoidal variation of the velocity with amplitude Δu and period P at the inner boundary $r_{\rm i}$ of the model. Thus, our models are defined by the prescription of the 4 fundamental stellar parameters ($T_\star$, $L_\star$, $M_\star$, $\epsilon_{\rm i}$) and of (P, Δu) to describe the interior pulsation. Details of the hydrodynamical modeling and the basic equations are given in Fleischer et al. (1992). For the determination of the equilibrium temperature the radiative transfer problem is solved in grey approximation in the hydrodynamical calculation, which does not yield the spectral energy distribution nor the lightcurves or the surface brightness profiles of the dust shell model. Therefore, in a second step, we solve the frequency–dependent stationary radiative transfer equation in spherical geometry for a given radial structure of the dust shell model, i.e. at a fixed instant of time. Details of the radiative transfer calculation are described in Winters et al. (1994a,b).

3 RESULTS

All results shown refer to *one* set of model parameters for which the best agreement with the observational data of **GL 3068** was achieved. The values of this set of parameters are

$L_\star$	=	13000 $L_\odot$
$T_\star$	=	2100 K
ϵ_C/ϵ_O	=	1.33
$M_\star$	=	0.9 $M_\odot$
P	=	696 d
Δu	=	8.0 km s^{-1}

which results in a calculated

- distance to **GL 3068** = 1.3 kpc
- final outflow velocity = 15.7 km s^{-1}
- mass loss rate = 1.7 10^{-4} $M_\odot$ yr^{-1}
- dust–to–gas ratio = 1.6 10^{-3}

The radial structure of the CDS for the model is shown in **Figure 1** at one instant of time. Similar to all our time–dependent models (as e.g. in Fleischer et al. 1992) several characteristic structures can be seen:

- the CDS exhibits a discrete or onion–like structure, i.e. the dust is not distributed homogeneously but in distinct layers. This can be seen, for instance, in the course of the degree of condensation f_c in the 2nd row of Fig. 1.

- these dust layers are spatially correlated with the hydrodynamical structure, e.g. the velocity, which suggests a common mechanism for their creation. Indeed, the process of *dust–amplified shocks* as described in detail in Fleischer et al. (1992) is also at work in this particular model.

- the radial structure of the temperature is characterized by a pronounced *back–warming effect*, i.e. the material closer to the star is heated due to blocking of the short wavelength radiation by the dust grains. This effect has a decisive influence on the dust nucleation process.

Figure 2 shows the spectral energy distribution at two selected instants of time. The upper diagram represents the spectrum at the first measured maximum at t = 2.25 P in Fig. 3, the lower diagram belongs to the second measured minimum at t = 3.80 P. Note that the IRAS– and submm–measurements were obtained at a fixed instant of time, i.e. they are the same in both plots.

Figure 3 shows the theoretical lightcurves at different wavelengths for a time interval of 7 pulsational periods. Near–IR observations by Le Bertre (1992) at $\lambda = 2.2\mu m$, $\lambda = 3.6\mu m$, and $\lambda = 4.8\mu m$ are shown as open triangles. In addition, in the upper left diagram, the luminosity of the model is plotted, which shows a strictly sinusoidal variation. Hence, the modulation in the lightcurves is caused by circumstellar effects. In fact, this model is *multiperiodic*, which in this case means, that a new dust layer is formed once each 3 pulsational periods. A hint for this time scale can be drawn from tracing the deep minima at long wavelengths (e.g. $\lambda = 200\mu m$). Note further, while going from short to long wavelengths, that there is an inversion in the behavior of the synthetic lightcurves, i.e. an increase in the mean magnitude at short wavelengths turns into a decrease at longer wavelengths, and vice versa.

The data by Le Bertre (1992) show that the lightcurves of GL 3068 cannot be approximated by a simple sine curve but that shifts in the mean magnitude are in fact observed for this object. Hence, the formation of discrete dust layers on time scales longer than the pulsational period, which is a natural consequence of the model calculation, offers the possibility of a physical explanation of this observed behavior.

Figure 4 shows the calculated intensity profiles $I(p)$ of the dust shell model (upper row), the integrated brightness profiles $b(p)$ (middle row) and the resulting visibility functions $V(q)$ (lower row) at different wavelengths for different instants of time. The first two instants of time are the same as in Fig. 2 at a maximum and a deep minimum of the lightcurve, respectively (cf. also Fig. 3). The third instant corresponds to a phase, when a new dust layer forms, and the last instant belongs to a phase of maximum optical depth of the dust shell, i.e. the new dust layer has completely developed.

At wavelengths larger than $\lambda \approx 5\mu$m, the current location of the dust layers is clearly indicated by steps in the brightness profiles or even by intermediate maxima in the intensity profiles at longer wavelengths (e.g. at $\lambda = 25\mu$m). These structures are caused by thermal emission of dust, concentrated in the discrete layers. A temporal evolution of the shell is also seen in the corresponding visibility functions, however the quantitative changes are less pronounced. Therefore, in order to obtain a further test of the model, it would be very valuable to observe the brightness distribution of GL 3068 directly with very high angular resolution (≈ 0.01 arcsec).

4 CONCLUSIONS

By the comparison of a consistent quantitative model for GL 3068 with respective observations we have demonstrated that our modeling approach is appropriate to describe the detailed structure of the circumstellar dust shell around this extreme carbon star. The results of our calculations provide a tool for the physical explanation of the characteristic properties found in rather different observed quantities.

Acknowledgments
This work was supported by the BMBF (grant 05 3BT13A 6) and by the DFG (grant Se 420/8–1).

5 REFERENCES

Bujarrabal V., Fuente A., Omont A., 1994, *A&A* 285, 247
Epchtein N., Le Bertre T., Lépine J. R. D., 1990, *A&A* 227, 83
Fleischer A. J., Gauger A., Sedlmayr E., 1992, *A&A* 266, 321
IRAS-Science-Team, 1986, *A&AS* 65, 607
Jones B., Merrill K. M., Puettner R. C., Willner S. P., 1978, *AJ* 83, 1437
Kastner J. H., Forveille T., Zuckerman B., Omont A., 1993, *A&A* 275, 163
Le Bertre T., 1992, *A&AS* 94, 377
Winters J. M., Dominik C., Sedlmayr E., 1994a, *A&A* 288, 255
Winters J. M., Fleischer A. J., Gauger A., Sedlmayr E., 1994b, *A&A* 290, 623

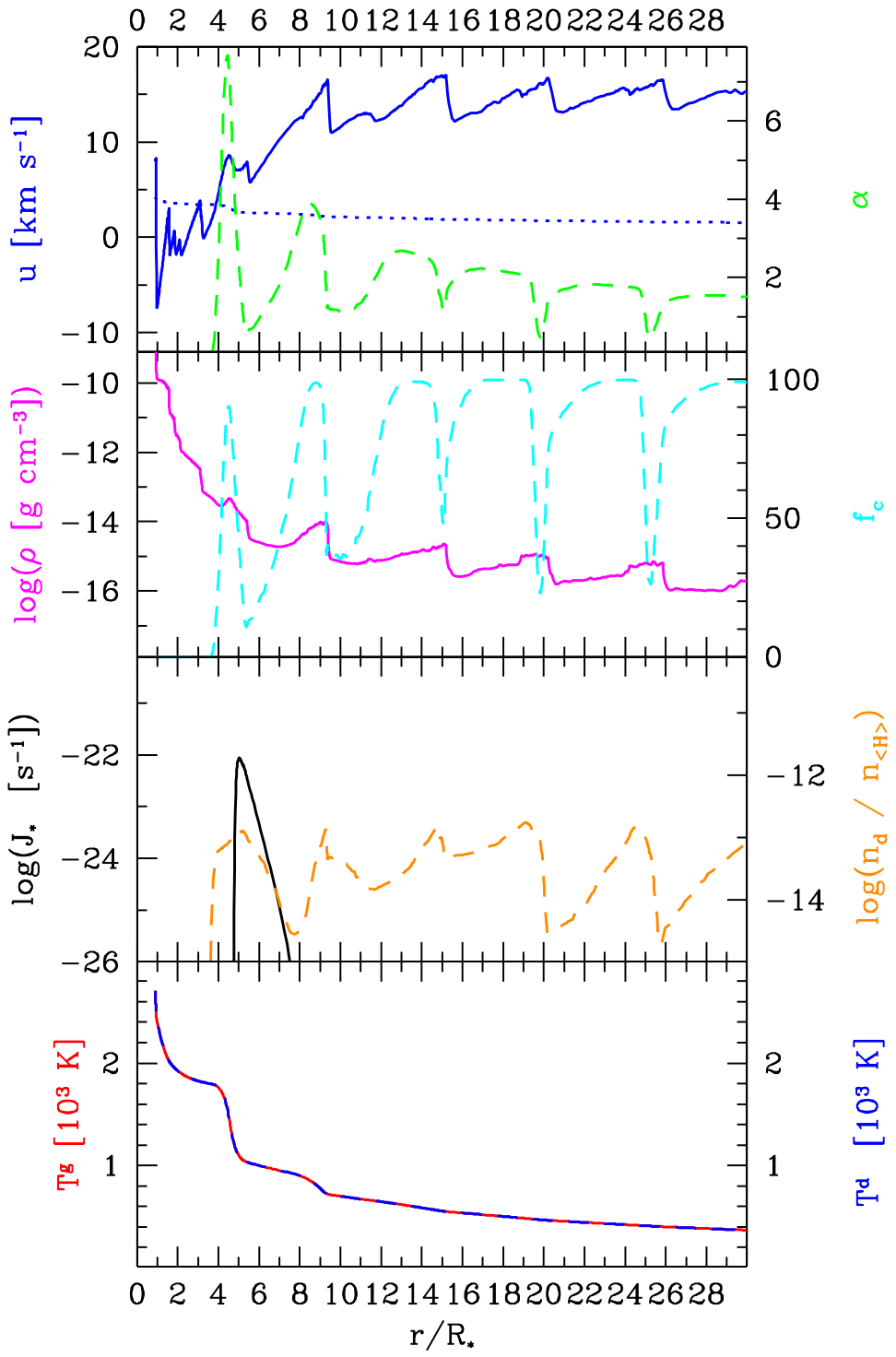

Figure 1: Radial structure of the CDS at the beginning of the hydrodynamical cycle. Shown are **upper diagram:** the velocity u (blue line), sound velocity (blue dashed), radiative acceleration in units of the gravitational acceleration α (green dashed), **2**nd **diagram:** the density ρ (solid red), the degree of condensation f_c (light blue dashed), **3**rd **diagram:** the nucleation rate J_* (solid black), the number of dust particles per H–atom $n_{\rm d}/n_{<\rm H>}$ (dashed brown), **lower diagram:** the gas temperature $T^{\rm g}$ (red), and the temperature in radiative equilibrium $T^{\rm d}$ (blue)

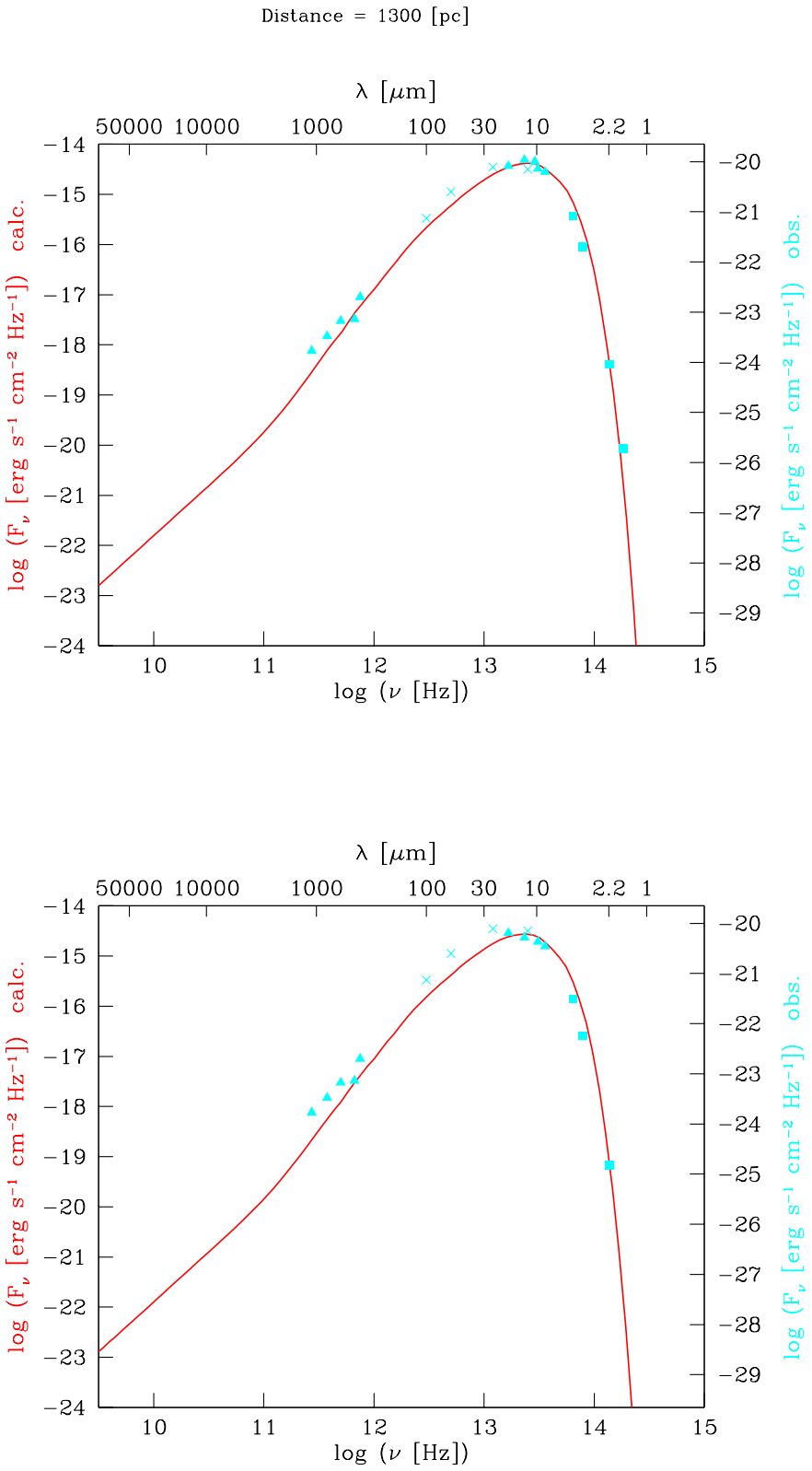

Figure 2: Theoretical spectrum of the dust shell model (red solid lines) at $t = 2.25P$ (upper diagram) and at $t = 3.80P$ (lower diagram), cf. Fig. 3, and observed spectrum of GL 3068 (blue symbols) at **maximum** phase of the lightcurve (upper diagram) and at **minimum** phase of the lightcurve (lower diagram).

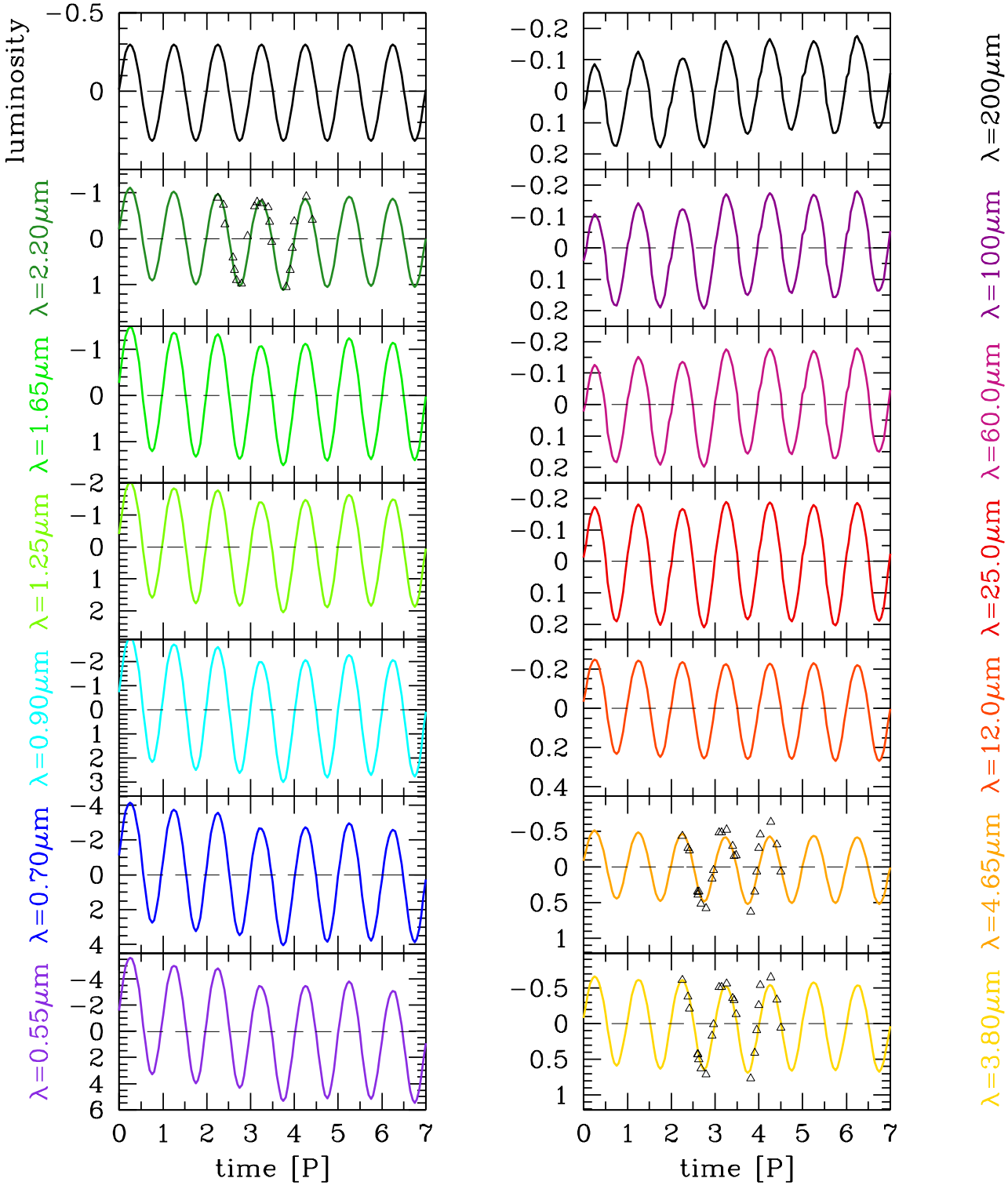

Figure 3: Theoretical lightcurves of the dust shell model (solid lines) at different wavelengths over a time interval of 7 pulsation periods and observed lightcurves of GL 3068 (black symbols at $\lambda = 2.20\mu$m (K), $\lambda = 3.60\mu$m (L), and $\lambda = 4.80\mu$m (M) (Le Bertre 1992)). The lightcurves are plotted in magnitudes normalized to the mean magnitude. Note the different scaling of the ordinate at different wavelengths.

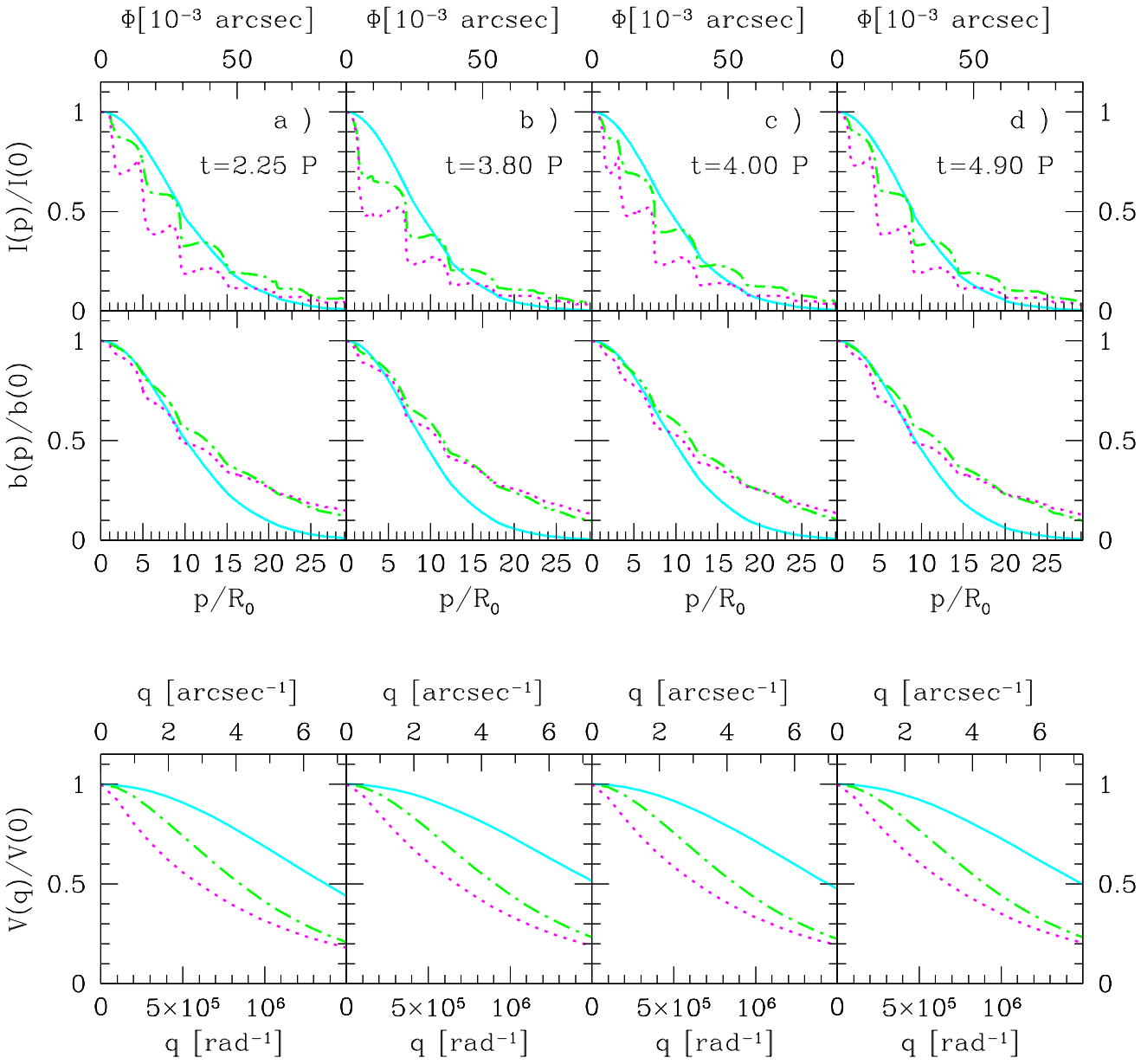

Figure 4: Intensity profiles (upper diagrams), integrated brightness distributions (second row), and visibilities (lower panel) of the dust shell model for $\lambda = 2.2\mu$m (solid blue lines), $\lambda = 12\mu$m (dash–dotted green lines), and $\lambda = 25\mu$m (dotted red lines) at different instants of time (cf. Fig. 3). A distance of $d = 1300\,$pc is assumed.